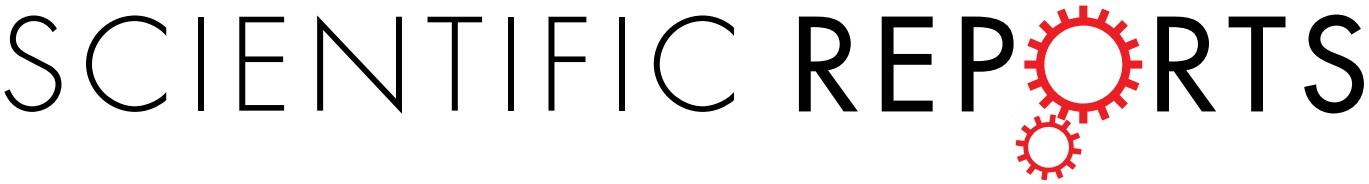

OPEN

Beyond Slurry-Cast Supercapacitor Electrodes: PAN/MWNT Heteromat-Mediated Ultrahigh Capacitance Electrode Sheets

Received: 08 August 2016
Accepted: 21 December 2016
Published: 31 January 2017

Jung Han Lee[1,*], Jeong A Kim[1,*], Ju-Myung Kim[1], Sun-Young Lee[2], Sun-Hwa Yeon[3] & Sang-Young Lee[1]

Supercapacitors (SCs) have garnered considerable attention as an appealing power source for forthcoming smart energy era. An ultimate challenge facing the SCs is the acquisition of higher energy density without impairing their other electrochemical properties. Herein, we demonstrate a new class of polyacrylonitrile (PAN)/multi-walled carbon tube (MWNT) heteromat-mediated ultrahigh capacitance electrode sheets as an unusual electrode architecture strategy to address the aforementioned issue. Vanadium pentoxide (V_2O_5) is chosen as a model electrode material to explore the feasibility of the suggested concept. The heteromat V_2O_5 electrode sheets are produced through one-pot fabrication based on concurrent electrospraying (for V_2O_5 precursor/MWNT) and electrospinning (for PAN nanofiber) followed by calcination, leading to compact packing of V_2O_5 materials in intimate contact with MWNTs and PAN nanofibers. As a consequence, the heteromat V_2O_5 electrode sheets offer three-dimensionally bicontinuous electron (arising from MWNT networks)/ion (from spatially reticulated interstitial voids to be filled with liquid electrolytes) conduction pathways, thereby facilitating redox reaction kinetics of V_2O_5 materials. In addition, elimination of heavy metallic foil current collectors, in combination with the dense packing of V_2O_5 materials, significantly increases (electrode sheet-based) specific capacitances far beyond those accessible with conventional slurry-cast electrodes.

Ongoing surge in demand for electric vehicles (EVs), stationary energy storage systems (ESSs), and flexible portable electronics relentlessly pushes us to develop advanced rechargeable power sources affording reliable electrochemical performance and safety tolerance[1,2]. Among numerous power sources reported to date, supercapacitors (SCs) have garnered a great deal of attention as an appealing system to fulfill the aforementioned requirements owing to their exceptional rate capability, cycle life, electrochemical reversibility, and safety[3–5]. These advantageous characteristics of SCs are believed to be well-suited particularly for EV battery applications[6–8]. However, the relatively low energy density of SCs, compared to those of other power sources such as lithium-ion batteries, has posed a formidable challenge to their versatile applications. Of various SC systems reported to date, metal oxide-based SCs are featured with reversible Faradaic redox reactions, thus enabling significant increase in capacitance[9–11]. Previous studies on the metal oxide SCs have been mostly devoted to synthesis and engineering of electrode active materials themselves[12–15], with a particular focus on improvement of their capacitance, electrical conductivity, and electrolyte accessibility.

Meanwhile, from the electrode architecture point of view, conventional electrodes are fabricated by slurry casting method, in which electrode active materials, carbon powder conductive additives, and polymer binders are simply piled up on top of metallic foil (or foam) current collectors[16,17]. Unfortunately, such a stereotypical electrode architecture often gives rise to nonuniform/sluggish transport of electrons and ions particularly in through-thickness direction of electrodes. Moreover, the inevitable use of heavy metallic foil current collectors has made it difficult for us to further increase energy density in a fixed electrode volume/weight. One promising way to resolve these issues

[1]Department of Energy Engineering, School of Energy and Chemical Engineering, Ulsan National Institute of Science and Technology (UNIST), Ulsan 689-798, Korea. [2]Department of Forest Products, Korea Forest Research Institute, Seoul 02455, Korea. [3]Energy Storage Lab., Korea Institute of Energy Research (KIER), Yuseong, Daejeon 305-343, Korea. *These authors contributed equally to this work. Correspondence and requests for materials should be addressed to S.-H.Y. (email: ys93@kier.re.kr) or S.-Y.L. (email: syleek@unist.ac.kr)

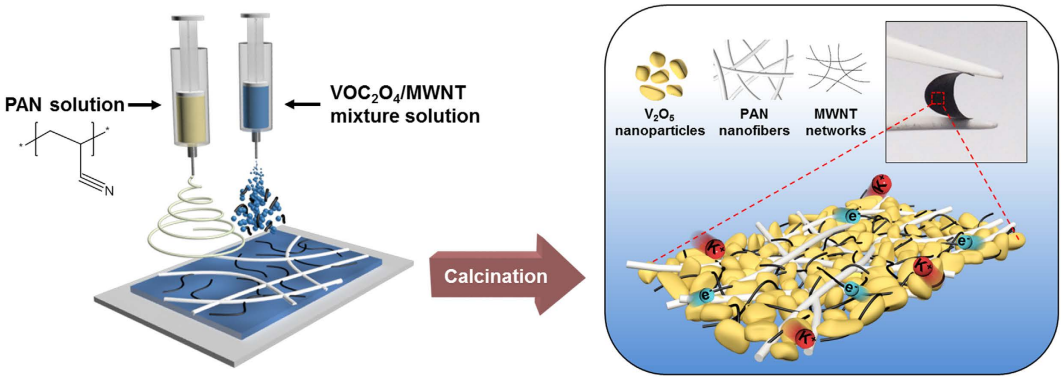

Figure 1. Schematic illustration showing the fabrication procedure and morphological uniqueness of heteromat V_2O_5 electrode sheets. The one-pot fabrication based on concurrent electrospraying (for V_2O_5 precursor/MWNT) and electrospinning (for PAN nanofiber) followed by calcination was depicted.

is the removal of heavy metallic current collectors in the electrodes. A number of studies have been reported for the development of metallic foil current collector-free electrodes for SCs[11,18,19] and also lithium-ion batteries[20–23]. However, most of these previous works have combined electrode materials with pre-formed three-dimensional (3D) porous scaffolds, thus resulting in low active-mass loading per unit electrode area.

Here, we present a new class of metallic foil current collector-free, polyacrylonitrile (PAN)/multi-walled carbon tube (MWNT) heteromat-mediated ultrahigh capacitance electrode sheets as an unusual electrode architecture strategy to address the aforementioned long-standing challenge of SC electrodes. As a proof-of-concept for this approach, vanadium pentoxide (V_2O_5) is chosen as a model electrode material. V_2O_5 has been investigated due to its natural abundance, low cost, and various oxidation states (V^{2+} to V^{5+}) suitable for realization of higher pseudo-capacitance[24–26]. However, V_2O_5 suffers from low electronic conductivity (10^{-2} to 10^{-3} S cm^{-1}), which remains a critical challenge to its application to SC electrodes.

The heteromat V_2O_5 electrode sheets presented herein are composed of densely-packed V_2O_5 materials in intimate contact with the MWNTs and the PAN nanofibers. The MWNTs offer highly-interconnected electronic networks and also serve as an alternative current collector. The PAN nanofibers act as a mechanically-reinforcing skeleton and also an one-dimensional (1D)-shaped electrode binder. Notably, the V_2O_5 electrode sheets are produced through one-pot fabrication based on concurrent electrospraying (for V_2O_5 precursor (=VOC_2O_4)/MWNT) and electrospinning (for PAN nanofiber) followed by calcination. Benefiting from the aforementioned material/architecture uniqueness, the heteromat V_2O_5 electrode sheets offer 3D bicontinuous electron/ion conduction pathways, thereby facilitating redox reaction kinetics of V_2O_5 materials. Moreover, the removal of heavy metallic foil current collectors, in association with compact packing of V_2O_5 materials, enables a remarkable increase in (electrode sheet-based) specific capacitances, which lie far beyond those achievable with conventional slurry-cast electrodes.

Results

One-pot fabrication and structural/physicochemical characterization of heteromat V_2O_5 electrode sheets. The self-standing, metallic foil current collector-free heteromat V_2O_5 electrode sheets were produced through the concurrent electrospraying (for V_2O_5 precursor (=VOC_2O_4)/MWNT) and electrospinning (for PAN nanofiber) followed by calcination in air. This one-pot fabrication procedure of the V_2O_5 electrode sheet, along with its morphological uniqueness, was schematically illustrated in Fig. 1.

The structure and physicochemical properties of the V_2O_5 electrode sheets were investigated as a function of calcination temperature (250 and 300 °C) that is expected to affect formation of amorphous or crystalline structure of the resulting V_2O_5 materials. The SEM images (Fig. 2a (surface) and b (cross-section)) of the V_2O_5 electrode sheet calcined at 250 °C (denoted as "V-250 electrode sheet") showed that the V_2O_5, MWNTs, PAN nanofibers are well mingled together and the thickness of the electrode sheet was approximately 28 μm. The V_2O_5 clusters were densely packed and in close contact with the electrosprayed MWNTs under the presence of PAN nanofibers. Meanwhile, the morphology of the V_2O_5 electrode sheet ("V-300 electrode sheet", thickness ~28 μm) calcined at 300 °C was characterized (Fig. 2d and e). A notable structural feature of the V-300 electrode sheet is the finely-dispersed V_2O_5 nanoparticles. This structural uniqueness of the V-250 and V-300 electrode sheets was further verified by analyzing TEM images (Supplementary Fig. S1). The MWNTs, together with the V_2O_5, were uniformly dispersed without serious aggregation, resulting in the highly interconnected electronic networks. In addition to the well-developed MWNT electronic networks, the spatially reticulated interstitial voids, which will be filled with electrolyte and thus act as ion-conducting pathways, were formed in the V-250 and V-300 electrode sheets. The difference in the V_2O_5 morphology between the two electrode sheets will be discussed in the following section, together with in-depth structural characterization.

Both the heteromat V_2O_5 electrode sheets exhibited the compact packing of V_2O_5 materials, which is anticipated to enable the realization of (electrode sheet-based) high specific capacitance. From the TGA result (Supplementary Fig. S2) and the selective etching of PAN (dimethylformamide (DMF) was used as an etching agent), the composition ratio of the V-250 and V-300 electrode sheets was estimated to be (V_2O_5/MWNT)/

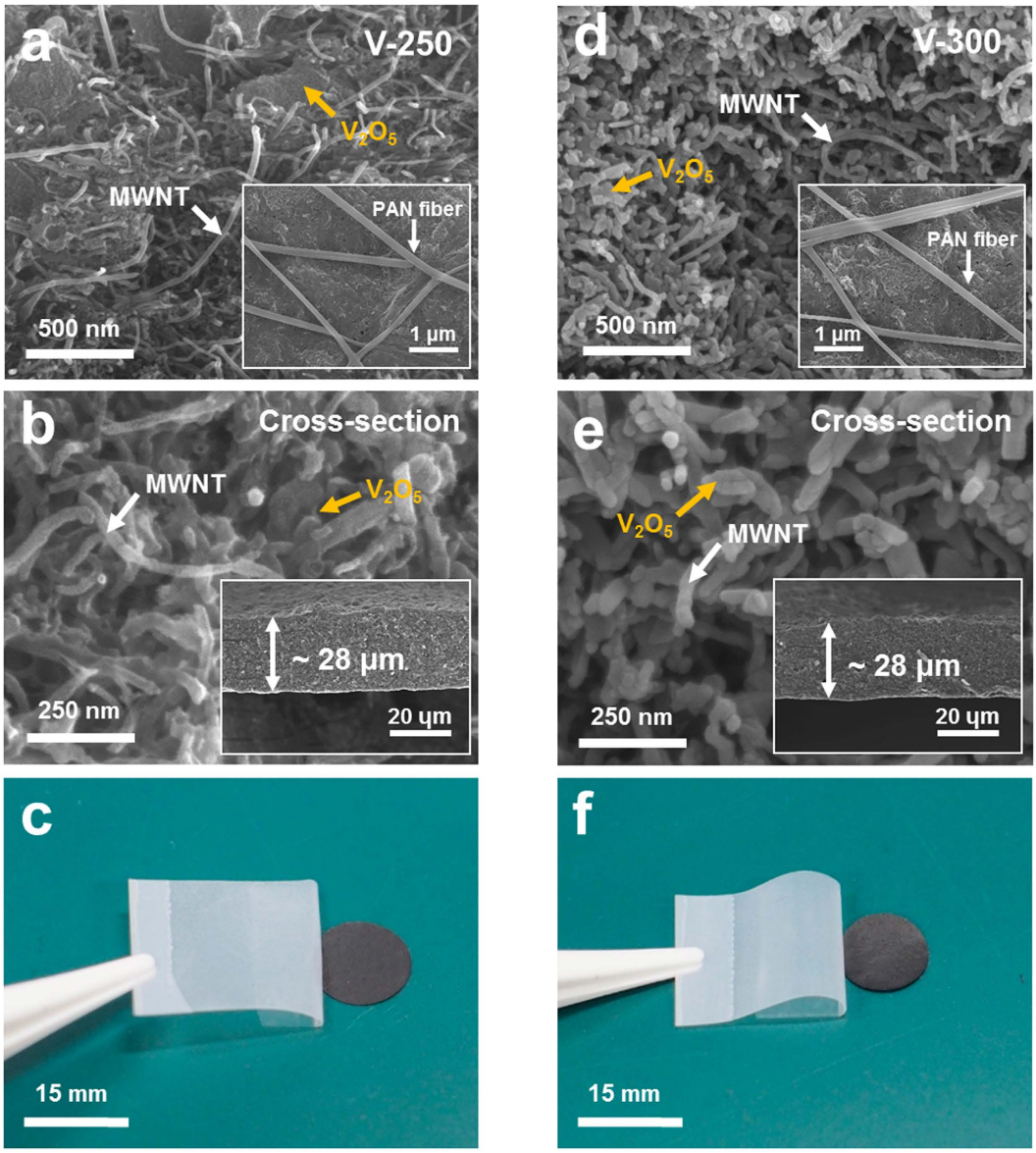

Figure 2. Morphological characterization of: (**a**–**c**) V-250 and (**d**–**f**) V-300 electrode sheets. (**a**,**d**) SEM images (surface) showing the good dispersion state of V_2O_5, MWNTs and PAN nanofibers, wherein insets are low-magnification view. (**b**,**e**) SEM images (cross-section). (**c**,**f**) A tape test using commercial 3 M scotch® tape.

PAN = (48/33)/19 (w/w/w). The effect of the composition ratio of the electrode sheets on their strucutre and electrochemical performance was examined. Below the MWNT content of 30 wt%, the resulting electrode sheets did not show significant improvement in the cell performance, which appeared similar to a control sample (fabricated through a conventional slurry cast method). Meanwhile, when the MWNT content was larger than 33 wt%, we failed to prepare V_2O_5/MWNT suspensions because electrospraying nozzles were frequently clogged. The structural robustness of the V-250 and V-300 electrode sheets was examined using peel-off test with 3 M scotch® tape. Neither detachment nor disintegration of the electrode components was observed for both electrodes (Fig. 2c and f), demonstrating that the V_2O_5 materials, MWNTs, and PAN nanofibers were tightly held together even in the absence of conventional polymer binders and metallic foil current collectors.

The one-pot synthesized V_2O_5 active materials in the V-250 and V-300 electrode sheets were characterized in more detail. Figure 3a shows XRD patterns of the V-250 and V-300 electrode sheets, along with those of control V_2O_5 nanoparticles (which were synthesized using the same VOC_2O_4 precursor and calcination condition employed for the V-300 electrode sheet). The control V_2O_5 nanoparticles showed the characteristic XRD peaks assigned to orthorhombic V_2O_5 with layered shcherbinaite structure ($Pmn2_1$)[27,28]. It is of note that the XRD peaks of the V_2O_5 in the V-300 electrode sheet appear well-matched with those of the control V_2O_5, verifying the synthesis of crystalline V_2O_5 materials in the V-300 electrode sheet. In comparison, no appreciable XRD peaks were observed at the V-250 electrode sheet, revealing the formation of amorphous V_2O_5 materials.

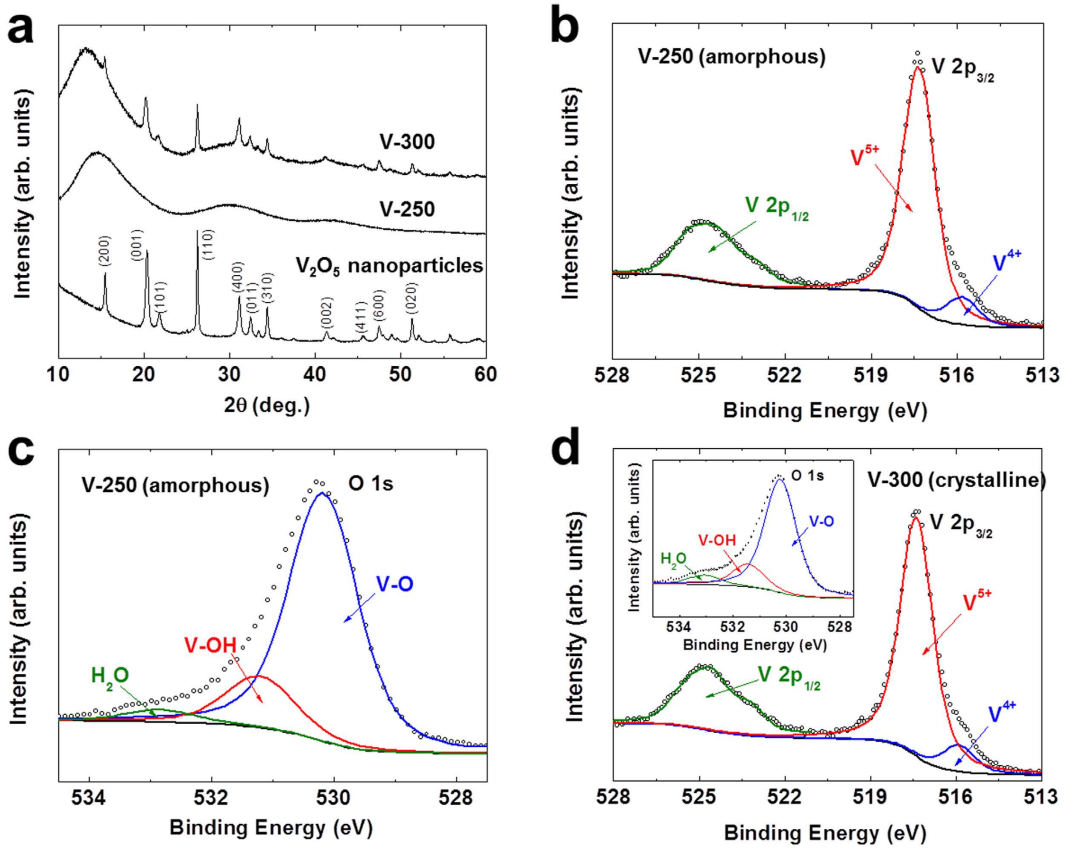

Figure 3. Structural (amorphous vs. crystalline) analysis of V-250 and V-300 electrode sheets. (**a**) XRD patterns showing the characteristic peaks ascribed to orthorhombic V_2O_5 with layered shcherbinaite structure ($Pmn2_1$). (**b**) XPS spectra showing the characteristic V $2p_{1/2}$ (525 eV) and V $2p_{3/2}$ (517 eV) peaks of V-250 electrode sheet. (**c**) XPS O 1 *s* peaks assigned to V-O (530 eV) and V-OH (531 eV) of V-250 electrode sheet. (**d**) XPS V $2p_{1/2}$ and V $2p_{3/2}$ peaks (an inset is O 1 *s* peaks) of V-300 electrode sheet.

The V_2O_5 materials in the V-250 and V-300 electrode sheets were further elucidated using XPS spectra. The characteristic V $2p_{1/2}$ (525 eV) and V $2p_{3/2}$ (517 eV) peaks[23,29] were observed at the V-250 electrode sheet (Fig. 3b). Intriguingly, the V $2p_{3/2}$ peaks were resolved into two contributions, V^{4+} and V^{5+}. The relatively higher intensity of the V^{5+} peaks indicates that a majority of the vanadium are V^{5+} state (i.e., corresponding to V_2O_5). In addition, the XPS O 1 *s* peaks[30] assigned to V-O (530 eV) and V-OH (531 eV) were detected at the V-250 electrode sheet (Fig. 3c). The aforementioned XPS spectra were also observed at the V-300 electrode sheet, demonstrating the presence of V_2O_5 materials (Fig. 3d). This structural characterization exhibits that the amorphous and crystalline V_2O_5 materials were successfully one-pot synthesized in the V-250 and V-300 electrode sheets, respectively.

An essential prerequisite to enable facile electrochemical reaction in rechargeable power sources is construction of well-developed electronic/ionic pathways. The electronic conductivity and electrolyte accessibility of the V-250 and V-300 electrode sheets were compared with those of a control V_2O_5 electrode sheet that was fabricated using a conventional slurry casting method (V_2O_5/carbon black additive/PVdF binder = 70/20/10 (w/w/w) on a Ni foil current collector, Supplementary Fig. S3). The V-250 electrode sheet presented the higher electronic conductivity (=4.4 S cm^{-1}, Supplementary Fig. S4a) than the control V_2O_5 electrode sheet (=1.3 S cm^{-1}). This facile electron conduction is attributed to the highly-interconnected MWNT electronic networks and the removal of conventional polymeric binders (that may partially shield V_2O_5 materials and conductive pathways). To check influence of the PAN nanofibers calcined at 300 °C on electronic conductivity, one control sheet solely comprising PAN nanofibers was fabricated. The PAN nanofiber sheet showed no detectable level of electronic conductivity (~0 S cm^{-1}) after the calcination at 300 °C in air, revealing that the PAN nanofibers themselves in the V-250 and V-300 electrode sheets would remain electronically inert.

The V-250 and V-300 electrode sheets showed the higher porosity (~29%) than the control V_2O_5 electrode sheet (~23%). Furthermore, the spatially reticulated interstitial void channels, in combination with the polar PAN nanofibers, facilitated capillary intrusion of liquid electrolyte (=2 M KCl aqueous electrolyte) into the V-250 and V-300 electrode sheets (Supplementary Fig. S4b), indicating the better electrolyte accessibility. These results demonstrate that the PAN/MWNT heteronanomat-mediated architecture of the V-250 and V-300 electrode sheets allowed for the construction of highly interconnected dual (i.e., electron/ion) conduction pathways, which is thus expected to boost up Faradaic redox reaction kinetics.

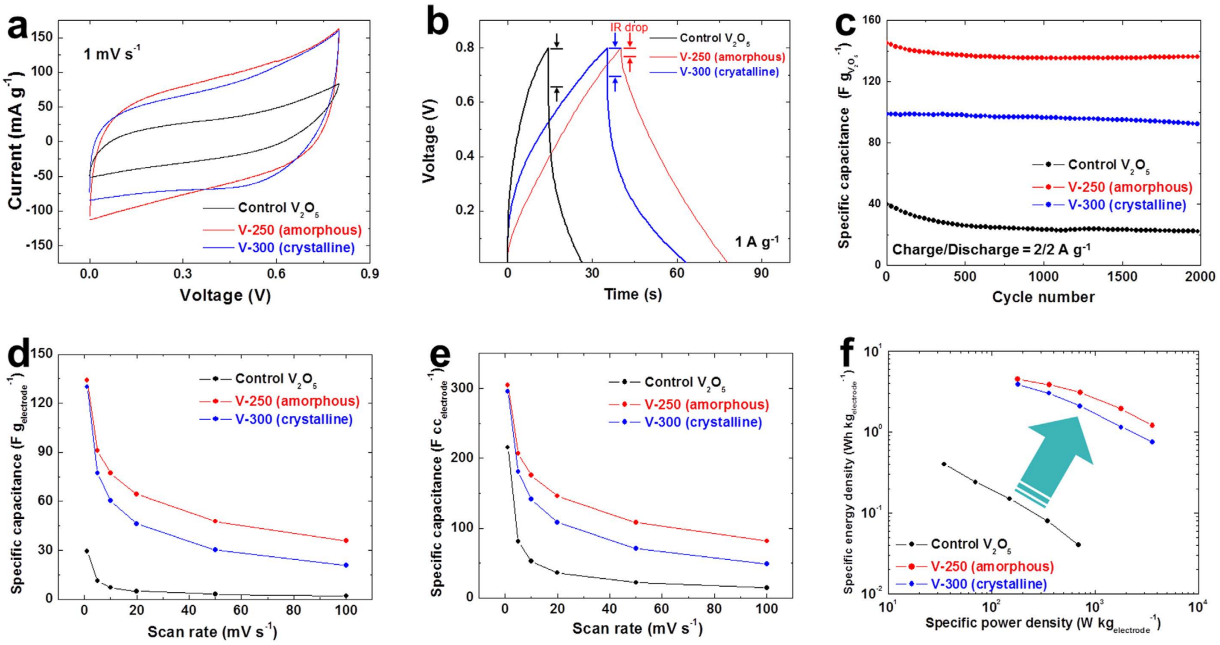

Figure 4. Electrochemical characterization of V-250, V-300, and control V_2O_5 electrode sheets. (**a**) Cyclic voltammetry (CV) curves (scan rate = 1 mV s^{-1}) showing typical Faradaic pseudocapacitive behavior. (**b**) Galvanostatic charge/discharge (GCD) profiles (current density = 1.0 A cm^{-2}). (**c**) Comparison in the cycling performance (up to 2,000 cycles) between the different electrode sheets at a current density of 2.0 A g^{-1}. (**d**) Comparison in the (electrode sheet-based) specific gravimetric capacitance (F $g_{electrode}^{-1}$) between the different electrode sheets as a function of scan rate (1–100 mV s^{-1}). (**e**) Comparison in the (electrode sheet-based) specific volumetric capacitance (F $cc_{electrode}^{-1}$) between the different electrode sheets as a function of scan rate (1–100 mV s^{-1}). (**f**) Ragone plots (specific gravimetric energy density (=Wh $kg_{electrode}^{-1}$) vs. specific gravimetric power density (=W $kg_{electrode}^{-1}$)) of SC cells, wherein the cell weight was determined by solely considering the electrode sheet weight.

Electrochemical characterization of heteromat V_2O_5 (V-250 and V-300) electrode sheets. The electrochemical performance of the V-250/V-300 electrode sheets was investigated with pouch-type symmetric cells (incorporating 2 M KCl aqueous electrolyte). The electrochemical reaction in V_2O_5 electrodes is can be expressed as follows[31]:

$$V_2O_5 + xK^+ + xe^- \leftrightarrow K_xV_2O_5, \quad (1)$$

wherein x is the mole fraction of reacted K^+ ions. The cyclic voltammetry (CV) curves (measured at a scan rate of 1 mV s^{-1}) showed typical Faradaic pseudocapacitive behavior (Fig. 4a). The V-250 electrode sheet presented the higher (V_2O_5 powder weight-based) specific gravimetric capacitance (=266 F g_{V2O5}^{-1}) than the V-300 (=259 F g_{V2O5}^{-1}) and the control V_2O_5 electrode sheet (=240 F g_{V2O5}^{-1}). This higher capacitance of the V-250 electrode sheet became more apparent with increasing scan rate (Supplementary Figs S5 and S6) To exactly estimate the specific gravimetric capacitance of V_2O_5 active materials, contribution of MWNTs themselves (Supplementary Fig. S7) was excluded.

The capacitance of SCs is known to depend on measurement condition (specifically, symmetric two-electrode vs. three-electrode configuration). Theoretically, the capacitance estimated from the three-electrode configuration is four times higher than that from the symmetric two-electrode system[4]. In addition, the three-electrode configuration tends to overestimate specific capacitances, while the two-electrode analysis shows opposite behavior[24]. It is of note that under the symmetric two-electrode configuration, the V-250 electrode sheet showed the higher specific gravimetric capacitance than previously reported V_2O_5/CNT composite electrodes (Supplementary Table S1)[32–35]. This excellence in the capacitance of the V-250 electrode sheet was further verified by conducting galvanostatic charge-discharge (GCD) tests. The symmetric triangular-shaped charge/discharge profiles were found at all the electrode sheets over a wide range of current densities (0.5–5.0 A g^{-1}) (Supplementary Fig. S8). The comparison in the GCD profiles (measured at 1.0 A g^{-1}) between the different electrode sheets (Fig. 4b) exhibited that the V-250 electrode sheet presented the smaller IR drop (=0.03 V) and longer charge/discharge time (=40/39 s) as compared to the control V_2O_5 electrode sheet (=0.15 V and 14/12 s) and the V-300 electrode sheet (=0.1 V and 34/30 s). Moreover, the higher capacitance of the V-250 electrode sheet was maintained over 2,000 charge/discharge cycles at a current density of 2.0 A g^{-1} (Fig. 4c), manifesting the long-term cycling stability. The superior electrochemical performance of the V-250/V-300 electrode sheets over the control V_2O_5 electrode sheet is due to the PAN/MWNT heteronanomat-mediated structural uniqueness that allows 3D-bicontinuous electron/ion conduction. Meanwhile, amorphous V_2O_5 materials are known to provide

higher capacitance than crystalline counterparts because their redox reaction occurs not only on the surface but also inside the bulk[5,26,36]. The aforementioned comparison in the specific gravimetric capacitance between the V-250 and V-300 electrode sheets appeared well consistent with the previously reported results.

It is again underlined that the V-250 electrode sheet does not contain heavy nickel (Ni) foil current collectors, which is thus anticipated to beneficially affect (electrode sheet-based) specific gravimetric/volumetric capacitance. The V-250 one showed the substantial reduction in the total areal weight, as compared to the control V_2O_5 electrode sheet (Supplementary Fig. S9). The areal active-mass loading (that exclusively considers the weight of V_2O_5 materials) of the V-250 electrode sheet ($=2.0\,mg\,cm^{-2}$) appeared negligibly different from that of the control V_2O_5 one ($=2.3\,mg\,cm^{-2}$), revealing that the lower weight of the V-250 electrode sheet is mainly due to the removal of the heavy Ni foil current collector ($=23\,mg\,cm^{-2}$). As a consequence, the V-250 electrode sheet exhibited the significant improvement in the specific gravimetric capacitance expressed as capacitance per electrode sheet weight ($=F\,g_{electrode}^{-1}$) (e.g., $134\,F\,g_{electrode}^{-1}$ at a scan rate of $1\,mV\,s^{-1}$) than the conventional V_2O_5 electrode sheet ($=29\,F\,g_{electrode}^{-1}$) over a wide range of scan rates (Fig. 4d). In addition, the increase in the specific volumetric capacitance expressed as capacitance per electrode sheet volume ($=F\,cc_{electrode}^{-1}$) was shown in Fig. 4e. The aforementioned superior electrochemical performance (shown in Fig. 4a–e) of the V-250 electrode sheet compared to the conventional V_2O_5 electrode sheet was further confirmed by the lower cell impedance (Supplementary Fig. S10), underscoring the advantageous effect of the PAN/MWNT heteromat electrode architecture on the cell performance. Notably, the V-250 and V-300 electrode sheets showed the significantly lower bulk resistance (at the highest frequency region) than the control V_2O_5 electrode sheet, demonstrating the more facilitated ion transport owing to their well-developed 3D continuous ion conduction channels.

The above-mentioned substantial improvement in the redox reaction kinetics (enabled by the PAN/MWNT heteronanomat-mediated 3D bicontinuous electron/ion conduction pathways) and the specific gravimetric/volumetric capacitance (enabled by the removal of heavy Ni foil current collectors and also dense packing of V_2O_5 materials) of the V-250 electrode sheet was further highlighted by analyzing the Ragone plot, in which the cell weight was determined by solely considering the electrode sheet weight. Figure 4f verified that the V-250 electrode sheet exhibited the remarkable increase in the (electrode sheet-based) specific gravimetric energy ($=Wh\,kg_{electrode}^{-1}$)/power ($=W\,kg_{electrode}^{-1}$) densities far beyond those accessible with the control V_2O_5 electrode sheet (fabricated by a conventional slurry casting method), underscoring its potential benefits as an exceptional high-energy/high-power density power source.

Discussion

In summary, we presented the metallic foil current collector-free, PAN/MWNT heteromat-mediated V_2O_5 ultrahigh capacitance electrode sheets for use in SCs. The heteromat V_2O_5 electrode sheets were produced through the concurrent electrospraying (for V_2O_5 precursor/MWNT) and electrospinning (for PAN nanofiber) followed by the calcination. Notably, this one-pot fabrication of the V_2O_5 electrode sheet (starting directly from V_2O_5 precursor) allowed for dense packing of the resulting V_2O_5 materials in close contact with the MWNTs and PAN nanofibers. The heteromat V_2O_5 electrode sheet calcined at 250 °C yielded the amorphous V_2O_5, thus providing the higher capacitance than the heteromat V_2O_5 electrode one calcined at 300 °C (containing the crystalline V_2O_5). Driven by the material/architecture uniqueness, the heteromat V_2O_5 electrode sheets offered the 3D bicontinuous electron/ion conduction pathways, eventually facilitating the redox reaction kinetics of V_2O_5 materials. Furthermore, the removal of heavy Ni foil current collectors, in association with the compact packing of V_2O_5 materials, substantially increased the (electrode sheet-based) specific gravimetric electrode capacitances (e.g., $134\,F\,g_{electrode}^{-1}$ for the V-250 electrode sheet vs. $29\,F\,g_{electrode}^{-1}$ for the control V_2O_5 electrode sheet, at a scan rate of $1\,mV\,s^{-1}$). As a consequence, the V_2O_5 electrode sheet enabled the shift of the specific energy/power densities to higher values in the Ragone plot, which lie far beyond those achievable with conventional slurry casting-based electrode technologies. The heteromat V_2O_5 electrode sheets based on the concept of "one-pot fabrication of electrode sheets directly from electrode material precursors" can be suggested as a facile and versatile platform technology (readily applicable to other electrode materials) and opens a new route towards high-energy/high-performance SC electrodes.

Methods

One-pot fabrication of PAN/MWNT heteromat-mediated V_2O_5 electrode sheets (directly from V_2O_5 precursors). The V_2O_5 electrode sheets were produced through one-pot fabrication based on the concurrent electrospraying (for VOC_2O_4 ($=V_2O_5$ precursor)/MWNT) and electrospinning (for PAN nanofiber) followed by calcination in air. Firstly, in order to prepare the VOC_2O_4/MWNT mixture solution, 0.5 g of V_2O_5 powders (Aldrich) and 1.2 g of oxalic acid (Aldrich) were dissolved in 20 mL distilled water at room temperature for 3 h, yielding the VOC_2O_4 solution. Subsequently, 0.25 g of MWNT (CNT150, Hanwha), 0.12 g of PVP (molecular weight = 55,000 g mol^{-1}, Aldrich), 20 mL of ethanol were added into the VOC_2O_4 solution under sonication. PAN (molecular weight = 150,000 g mol^{-1}, Aldrich) was dissolved in dimethylformamide (DMF) at 80 °C for 12 h to prepare 10 wt.% PAN solution. The VOC_2O_4/MWNT and the PAN solutions were subjected to concurrent electropraying/electrospinning through different nozzles at room temperature. The working voltages/ejection rates were 10/10 (kV/μL min^{-1}) for the electrospinning and 20/120 (kV/μL min^{-1}) for the electrospraying, respectively. The resulting mixture mat was dried at 80 °C for 24 h and then heat-treated in air at 250 or 300 °C for 5 h to allow calcination of V_2O_5 directly inside the mixture mat, leading to a self-standing V_2O_5 electrode sheet. To prepare a control electrode sheet, bulk V_2O_5 nanoparticles were synthesized using the same VOC_2O_4 solution and the calcination process (300 °C for 5 h). The synthesized V_2O_5 nanoparticles were mixed with carbon black additives and polyvinylidene fluoride (PVdF) binder on a Ni foil current collector. The composition ratio of the control electrode sheet was V_2O_5/carbon black additive/PVdF binder = 70/20/10 (w/w/w).

Structural characterization of heteromat V_2O_5 electrode sheets. The morphology of the heteromat V_2O_5 electrode sheet was investigated using field emission scanning electron microscopy (FE-SEM) (S-4800, Hitachi). The amorphous/crystalline phases of V_2O_5 materials in the cathode sheet were analyzed by X-ray diffraction (XRD) (D/MAZX 2500 V/PC) measurement using Cu Kα radiation. The composition ratio of the V_2O_5 electrode sheet was determined from thermogravimetric analysis (TGA) measurement (SDT Q600, TA Instruments) at a heating rate of 10 °C min^{-1} under air atmosphere. The electronic conductivity of the V_2O_5 electrode sheet was examined using 4-point probe point technique (CMT-SR1000N, Advanced Instrument Technology). The surface structure of the V_2O_5 electrode sheet was elucidated by X-ray photoelectron spectroscopy (XPS) (ThermoFisher) with focused monochromatized Al Kα radiation. The porosity of the V_2O_5 electrode sheets was estimated by measuring its density difference before and after solvent (n-butanol) uptake[37].

Electrochemical performance of heteromat V_2O_5 electrode sheets. The electrochemical performance of the heteromat V_2O_5 electrode sheet was characterized using a pouch-type symmetric cell, in which the V_2O_5 electrode sheet was assembled with a polypropylene (PP) separator (Celgard 3501) and 2 M KCl aqueous electrolyte. The cyclic voltammetry (CV), galvanostatic charge-discharge (GCD) and electrochemical impedance spectroscopy (EIS) measurements of the V_2O_5 electrode sheet were performed with a potentiostat/galvanostat (VSP classic, Bio-Logic).

References

1. Armand, M. & Tarascon, J.-M. Building better batteries. *Nature* **451,** 652–657 (2008).
2. Larcher, D. & Tarascon, J.-M. Towards greener and more sustainable batteries for electrical energy storage. *Nat. Chem.* **7,** 19–29 (2015).
3. Simon, P. & Gogotsi, Y. Materials for electrochemical capacitors. *Nat. Mater.* **7,** 845–854 (2008).
4. Zhang, S. & Pan, N. Supercapacitors performance evaluation. *Adv. Energy Mater.* **5,** 1401401 (2015).
5. Wang, G., Zhang, L. & Zhang, J. A review of electrode materials for electrochemical supercapacitors. *Chem. Soc. Rev.* **41,** 797–828 (2012).
6. Jiang, J. *et al.* Recent Advances in metal oxide-based electrode architecture design for electrochemical energy storage. *Adv. Mater.* **24,** 5166–5180 (2012).
7. Xu, Y. *et al.* A metal-free supercapacitor electrode material with a record high volumetric capacitance over 800 F cm^{-3}. *Adv. Mater.* **27,** 8082–8087 (2015).
8. Fang, H.-T., Liu, M., Wang, D.-W., Ren, X.-H. & Sun, X. Fabrication and supercapacitive properties of a thick electrode of carbon nanotube–RuO_2 core–shell hybrid material with a high RuO_2 loading. *Nano Energy* **2,** 1232–1241 (2013).
9. Aravindan, V., Gnanaraj, J., Lee, Y.-S. & Madhavi, S. Insertion-type electrodes for nonaqueous Li-ion capacitors. *Chem. Rev.* **114,** 11619–11635 (2014).
10. Wei, W., Cui, X., Chen, W. & Ivey, D. G. Manganese oxide-based materials as electrochemical supercapacitor electrodes. *Chem. Soc. Rev.* **40,** 1697–1721 (2011).
11. Liao, Q., Li, N., Jin, S., Yang, G. & Wang, C. All-solid-state symmetric supercapacitor based on Co_3O_4 nanoparticles on vertically aligned graphene. *ACS Nano* **9,** 5310–5317 (2015).
12. Augustyn, V., Simon, P. & Dunn, B. Pseudocapacitive oxide materials for high-rate electrochemical energy storage. *Energy Environ. Sci.* **7,** 1597–1614 (2014).
13. Wang, Y. *et al.* Reduced mesoporous Co_3O_4 nanowires as efficient water oxidation electrocatalysts and supercapacitor electrodes. *Adv. Energy Mater.* **4,** 1400696 (2014).
14. Wang, P. *et al.* Carbon/carbon nanotube-supported RuO_2 nanoparticles with a hollow interior as excellent electrode materials for supercapacitors. *Nano Energy* **15,** 116–124 (2015).
15. Chou, J.-C. *et al.* RuO_2/MnO_2 core–shell nanorods for supercapacitors. *J. Mater. Chem. A* **1,** 8753 (2013).
16. Tarascon, J.-M. & Armand, M. Issues and challenges facing rechargeable lithium batteries. *Nature* **414,** 359–367 (2001).
17. Whittingham, M. S. Lithium batteries and cathode materials. *Chem. Rev.* **104,** 4271–4302 (2004).
18. Ye, G. *et al.* 3D reduced graphene oxide coated V_2O_5 nanoribbon scaffolds for high-capacity supercapacitor electrodes. *Part. Part. Syst. Charact.* **32,** 817–821 (2015).
19. Foo, C. Y., Sumboja, A., Tan, D. J. H., Wang, J. & Lee, P. S. Flexible and highly scalable V_2O_5-rGO electrodes in an organic electrolyte for supercapacitor devices. *Adv. Energy Mater.* **4,** 1400236 (2014).
20. Chao, D. *et al.* A V_2O_5/conductive-polymer core/shell nanobelt array on three-dimensional graphite foam: A high-rate, ultrastable, and freestanding cathode for lithium-ion batteries. *Adv. Mater.* **26,** 5794–5800 (2014).
21. Chen, X. *et al.* MWCNT/V_2O_5 core/shell sponge for high areal capacity and power density Li-ion cathodes. *ACS Nano* **6,** 7948–7955 (2012).
22. Lee, J. W. *et al.* Extremely stable cycling of ultra-thin V_2O_5 nanowire–graphene electrodes for lithium rechargeable battery cathodes. *Energy Environ. Sci.* **5,** 9889–9894 (2012).
23. Sun, Y. *et al.* A composite film of reduced graphene oxide modified vanadium oxide nanoribbons as a free standing cathode material for rechargeable lithium batteries. *J. Power Sources* **241,** 168–172 (2013).
24. Boukhalfa, S., Evanoff, K. & Yushin, G. Atomic layer deposition of vanadium oxide on carbon nanotubes for high-power supercapacitor electrodes. *Energy Environ. Sci.* **5,** 6872–6879 (2012).
25. Pan, X. *et al.* Fast supercapacitors based on graphene-bridged V_2O_3/VO_x core–shell nanostructure electrodes with a power density of 1 MW kg^{-1}. *Adv. Mater. Interfaces* **1,** 1400398 (2014).
26. Lee, H. Y. & Goodenough, J. B. Ideal supercapacitor behavior of amorphous $V_2O_5{\cdot}nH_2O$ in potassium chloride (KCl) aqueous solution. *J. Solid State Chem.* **148,** 81–84 (1999).
27. Cheah, Y. L., Aravindan, V. & Madhavi, S. Electrochemical lithium insertion behavior of combustion synthesized V_2O_5 cathodes for lithium-ion batteries. *J. Electrochem. Soc.* **159,** A273–A280 (2012).
28. Armstrong, M. J. *et al.* Carbon nanocage supported synthesis of V_2O_5 nanorods and V_2O_5/TiO_2 nanocomposites for Li-ion batteries. *J. Mater. Chem. A* **1,** 12568–12578 (2013).
29. Li, Z. *et al.* Interpenetrating network V_2O_5 nanosheets/carbon nanotubes nanocomposite for fast lithium storage. *RSC Adv.* **4,** 46624–46630 (2014).
30. Cao, Z. & Wei, B. V_2O_5/single-walled carbon nanotube hybrid mesoporous films as cathodes with high-rate capacities for rechargeable lithium ion batteries. *Nano Energy* **2,** 481–490 (2013).
31. Nagaraju, D. H., Wang, Q., Beaujuge, P. & Alshareef, H. N. Two-dimensional heterostructures of V_2O_5 and reduced graphene oxide as electrodes for high energy density asymmetric supercapacitors. *J. Mater. Chem. A* **2,** 17146–17152 (2014).
32. Saravanakumar, B., Purushothaman, K. K. & Muralidharan, G. V_2O_5/functionalized MWCNT hybrid nanocomposite: the fabrication and its enhanced supercapacitive performance. *RSC Adv.* **4,** 37437–37445 (2014).

33. Yilmaz, G., Guo, C. X. & Lu, X. High-performance solid-state supercapacitors based on V_2O_5/carbon nanotube composites. *ChemElectroChem* **3,** 158–164 (2016).
34. Singh, A. & Chandra, A. Significant performance enhancement in asymmetric supercapacitors based on metal oxides, carbon nanotubes and neutral aqueous electrolyte. *Sci. Rep.* **5,** 15551 (2015).
35. Shakir, I. *et al.* Ultra-thin and uniform coating of vanadium oxide on multiwall carbon nanotubes through solution based approach for high-performance electrochemical supercapacitors. *Electrochimica Acta* **111,** 400–404 (2013).
36. Uchaker, E. *et al.* Better than crystalline: amorphous vanadium oxide for sodium-ion batteries. *J. Mater. Chem. A* **2,** 18208–18214 (2014).
37. Choi, K.-H. *et al.* Heterolayered, one-dimensional nanobuilding block mat batteries. *Nano Lett.* **14,** 5677–5686 (2014).

Acknowledgements

This work was supported by Basic Science Research Program through the National Research Foundation of Korea (NRF) funded by the Ministry of Science, ICT and Future Planning (2015R1A2A1A01003474), wearable platform materials technology center (WMC) (2016R1A5A1009926), energy efficiency and resources R&D program (20112010100150), Korea Forest Research Institute (FP 0400-2016-01), and development program of the Korea Institute of Energy Research (KIER) (Grant No. B6-2432). This work was also financially supported by Batteries R&D of LG Chem.

Author Contributions

J.H.L. performed the experiments and analyzed the data. J.A.K. and J.-M.K. performed the electrochemical analysis. S.-H.Y. and S.-Y.L. commented on the experimental results. S.-Y.L. coordinated and supervised the overall project. J.H.L. and S.-Y.L. wrote the manuscript and all authors discussed the results and participated in manuscript preparation.

Additional Information

Supplementary information accompanies this paper at http://www.nature.com/srep

Competing financial interests: The authors declare no competing financial interests.

How to cite this article: Lee, J. H. *et al.* Beyond Slurry-Cast Supercapacitor Electrodes: PAN/MWNT Heteromat-Mediated Ultrahigh Capacitance Electrode Sheets. *Sci. Rep.* **7**, 41708; doi: 10.1038/srep41708 (2017).

Publisher's note: Springer Nature remains neutral with regard to jurisdictional claims in published maps and institutional affiliations.